

Ferrimagnetic 120° magnetic structure in Cu_2OSO_4

Virgile Yves Favre,¹ Gregory S. Tucker,^{1,2} Clemens Ritter,³ Romain Sibille,² Pascal Manuel,⁴ Matthias D. Frontzek,⁵ Markus Kriener,⁶ Lin Yang,^{1,7} Helmut Berger,⁸ Arnaud Magrez,⁸ Nicola P. M. Casati,⁹ Ivica Živković,^{1,*} and Henrik M. Rønnow^{1,†}

¹Laboratory for Quantum Magnetism, Institute of Physics,
Ecole Polytechnique Fédérale de Lausanne, CH-1015 Lausanne, Switzerland

²Laboratory for Neutron Scattering, Paul Scherrer Institut, CH-5232 Villigen PSI, Switzerland

³Institute Laue Langevin, BP 156, 38042, Grenoble, France.

⁴ISIS Facility, STFC Rutherford Appleton Laboratory, Oxfordshire OX11 0QX, UK

⁵Neutron Scattering Division, Oak Ridge National Laboratory, Oak Ridge, Tennessee 37830, USA

⁶RIKEN Center for Emergent Matter Science, Wako 351-0198, Japan.

⁷Laboratory of Physics of Complex Matter, Institute of Physics,
Ecole Polytechnique Fédérale de Lausanne, CH-1015 Lausanne, Switzerland

⁸Crystal Growth Facility, Ecole Polytechnique Fédérale de Lausanne, Lausanne, Switzerland.

⁹Swiss Light Source, Paul Scherrer Institut, 5232, Villigen, Switzerland

(Dated: October 9, 2020)

We report magnetic properties of a $3d^9$ (Cu^{2+}) magnetic insulator Cu_2OSO_4 measured on both powder and single crystal. The magnetic atoms of this compound form layers, whose geometry can be described either as a system of chains coupled through dimers or as a Kagomé lattice where every 3rd spin is replaced by a dimer. Specific heat and DC-susceptibility show a magnetic transition at 20 K, which is also confirmed by neutron scattering. Magnetic entropy extracted from the specific heat data is consistent with a $S = 1/2$ degree of freedom per Cu^{2+} , and so is the effective moment extracted from DC-susceptibility. The ground state has been identified by means of neutron diffraction on both powder and single crystal and corresponds to a ~ 120 degree spin structure in which ferromagnetic intra-dimer alignment results in a net ferrimagnetic moment. No evidence is found for a change in lattice symmetry down to 2 K. Our results suggest that Cu_2OSO_4 represents a new type of model lattice with frustrated interactions where interplay between magnetic order, thermal and quantum fluctuations can be explored.

I. INTRODUCTION

Materials with antiferromagnetic Heisenberg interactions between spins on a triangular lattice¹⁻³ inherently exhibit large frustration, resulting in many similar energy states giving rise to novel behavior. In practice, there exist several ways to build a full lattice from triangular motifs. The notion of quantum spin liquid was introduced in the form of the Resonating Valence Bond, as a potential ground state of the simple triangular lattice^{4,5} system. Later developments evidenced that both classical and quantum ground state of the triangular lattice actually displayed long range order in the so-called 120° configuration⁶. Among an intense search for quantum spin liquids in models and materials^{7,8}, considerable attention has been devoted experimentally⁹⁻¹², and theoretically¹³⁻¹⁵ to the so-called Kagomé lattice, which is obtained by removing 1/4 of the spins from a triangular lattice, leading a lower connectivity of four nearest neighbors instead of six, which enhances fluctuations. It has been argued theoretically that the $S = 1/2$ Kagomé Heisenberg antiferromagnet shows a spin-liquid ground state¹⁶⁻¹⁸ and it is still debated whether the resulting states should be gapped or not¹⁹⁻²¹.

Many experimental attempts have been made to find compounds hosting this rich Kagomé physics²²⁻²⁶. Herbertsmithite²⁷ remains one of the best candidates. Many other candidates exhibited deviations from the Kagomé model, such as: magnetic interactions that go beyond nearest neighbor²⁸; non-negligible out-of-plane coupling; a significant antisymmetric Dzyaloshinskii-Moriya (DM)

interaction^{29,30}, structural distortions or chemical disorder. These perturbations lift the degeneracy of an ideal spin-liquid and drive the system towards long-range magnetic order.

A major question that currently has no clear answer is to which extent quantum spin liquid properties can survive and co-exist with ordered states. This question extends beyond Kagomé related systems³¹. It is therefore interesting to study other triangle-containing lattice geometries than the pure triangular and Kagomé lattices.

In this context we present the study of Cu_2OSO_4 ³², which hosts a quasi-2D lattice built from triangular motifs. One way to describe the lattice is that of a Kagomé lattice with one third of the sites replaced by $S = 1/2$ pairs (dimers). Another way to characterize it would be chains coupled through spin pairs in a triangular frustrated pattern. As shall be presented below, the spin-pair appear ferromagnetically aligned, such that an effective model for the system could be described as a Kagomé lattice with $S = 1/2$ on 2/3 of the sites and $S = 1$ on 1/3 of the sites. No single crystal growth of Cu_2OSO_4 has previously been reported³³. Studies of powder samples of Cu_2OSO_4 ^{34,35} reported the DC susceptibility of the compound and showed evidence of a transition to a magnetically long range ordered state at 20 K. The DM interaction in the sample was estimated by the means of Electron Spin Resonance (ESR)³⁶. From bulk measurements, a non-collinear antiferromagnetic ground state was proposed³⁷. Here we report single crystal growth and the details of the ground state of Cu_2OSO_4 , derived from DC-susceptibility, magnetization, heat capacity, as well as x-ray and neutron scattering.

II. EXPERIMENTAL DETAILS

Single crystals of Cu_2OSO_4 were grown by chemical vapor transport. High quality Cu_2OSO_4 powder was synthesized using anhydrous CuSO_4 as a source in a quartz crucible placed in the center of a muffle furnace and heated at 740°C . Two different transport agents were placed in a quartz ampoule at room temperature: Cl_2 and NiBr_2 , as well as a portion of the Cu_2OSO_4 powder. The ampoules were placed in a two zone gradient furnace. The best charge and growth-zone temperatures were 650°C and 550°C respectively. After five weeks, several dark-brown, semitransparent crystals were obtained. The typical dimensions of the crystals are $4 \times 2 \times 0.5 \text{ mm}^3$. On most of the crystals the b axis can be identified as an edge and most of them also present a (001) facet.

Specific heat was measured using a physical properties measurement system (PPMS, Quantum Design, Inc) and magnetization was measured using both PPMS and a magnetic properties measurement system (MPMS, Quantum Design, Inc). Neutron diffraction experiments were performed on WAND, ZEBRA, D20 and WISH beam lines at ORNL, PSI, ILL and ISIS respectively. The measurement on D20 was done using the high resolution option with takeoff angle 90° and a wavelength of 2.41 \AA . 4 hour measurements were taken at 1.5 K and at 30 K while the temperature ramp was done between 1.5 K and 30 K using 30 min runs with about 0.45 K between consecutive runs. Synchrotron x-ray diffraction was performed at the MS-X04SA beam line³⁸ at SLS, PSI. For powder diffraction, crushed single crystals were used to minimize impurities.

III. RESULTS

A. X-ray diffraction and crystal structure

According to a previous study³², the compound belongs to the monoclinic space group $C 2/m$ with lattice parameters $a = 9.355(10) \text{ \AA}$, $b = 6.312(5) \text{ \AA}$, $c = 7.628(5) \text{ \AA}$, $\alpha = \gamma = 90^\circ$, and $\beta = 122.29^\circ$.

To determine the temperature dependence of the nuclear structure, we performed temperature dependent x-ray diffraction on a powder sample. The temperature dependence of lattice parameters was extracted from LeBail fits (LBF) and is shown in Fig. 1, as well as the unit cell volume. The overall thermal contraction of the lattice has been observed down to 50 K, with a minimum of lattice parameters a and b around 60 K. This non-monotonic temperature dependence could be due to the onset of magnetic correlations coupling to the lattice. Similar magneto-elastic coupling is observed below the ordering temperature (Fig. 2).

The crystal structure of Cu_2OSO_4 gives rise to an interesting magnetic lattice. The copper atoms occupy two inequivalent positions. They are arranged in the ab-plane, with atoms on copper site one (Cu_1) exactly in the plane, while atoms of copper site two (Cu_2) are positioned symmetrically above and below the plane. Fig. 3(a) shows how the planes are then interconnected through SO_4 tetrahedra³⁹. The arrangement of Cu_1 and Cu_2 ions in the quasi-2D planes can be described either as

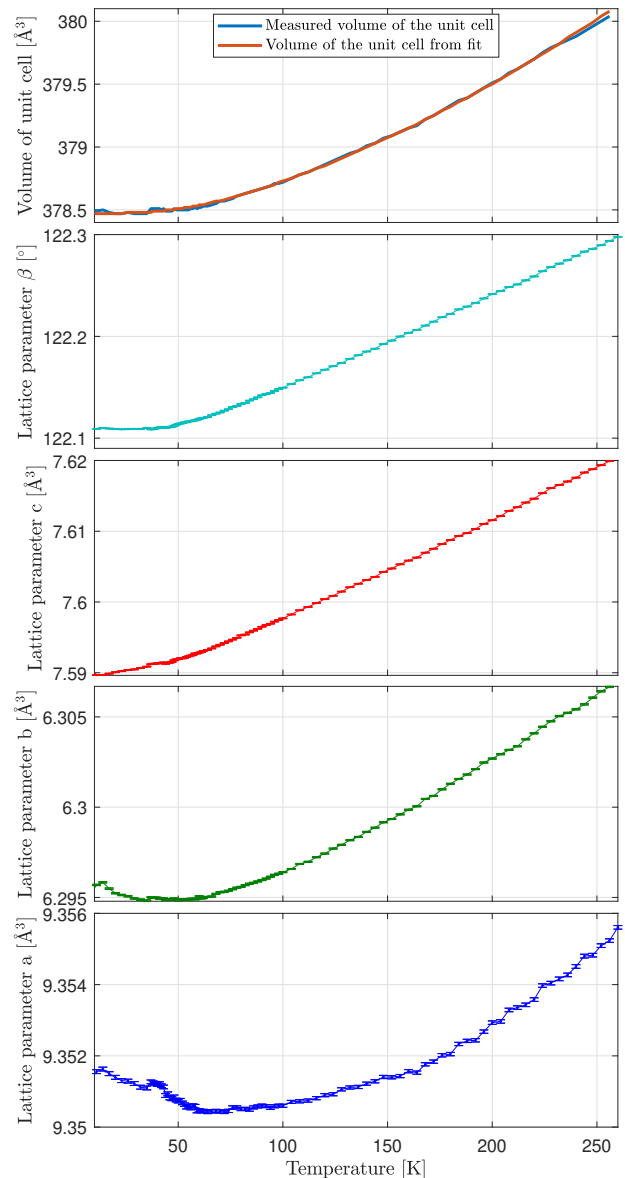


FIG. 1. Change in lattice parameters and unit cell volume obtained from LeBail fitting of powder x-ray diffraction data.

Cu_1 chains along the crystallographic b-axis, interconnected by Cu_2 dimers in a frustrated zig-zag pattern; or it can be described as a Kagomé lattice with one third of the sites replaced by dimers, or it can be viewed as Cu_1 chains coupled through Cu_2 dimers. Fig. 3(b) illustrate how viewing the magnetic layers rotated 8.5° around the b-axis plane overlays the Cu_2 ions resulting in the familiar Kagomé motif. Fig. 9 show the magnetic lattice viewed directly along c^* .

B. Specific Heat

The specific heat C_p measured from 2 K to 200 K in zero field and in a magnetic field of 9 T is shown in Fig. 4. The C_p above 70 K for both fields is essentially the same, increas-

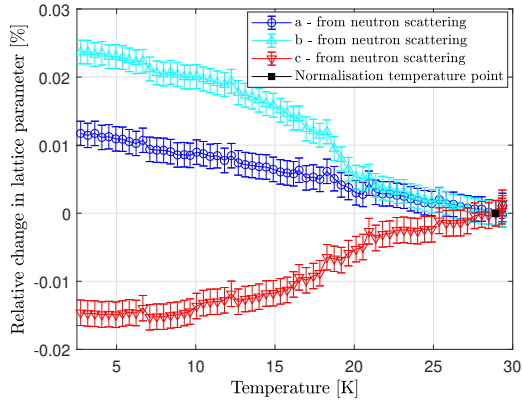


FIG. 2. Relative changes in lattice parameters obtained from neutron diffraction. The data has been normalized to data measured at 29 K (black square).

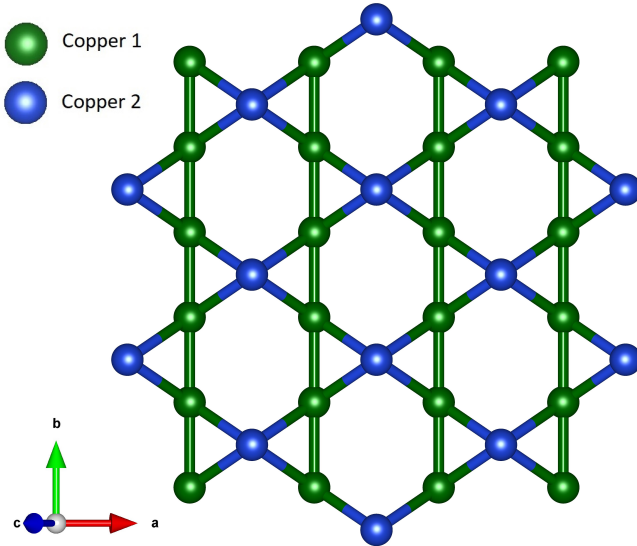
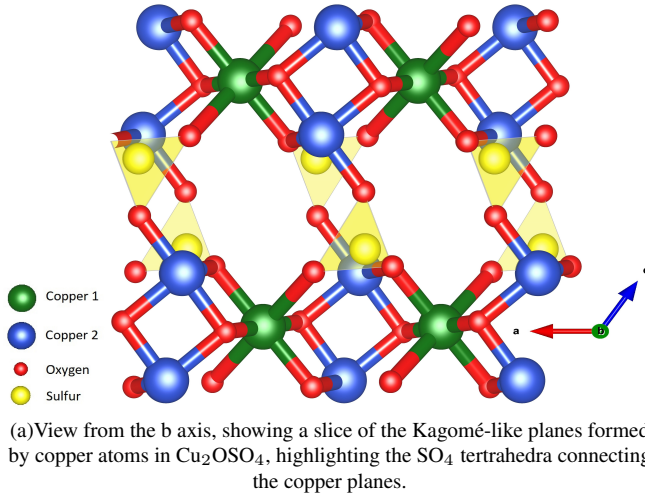


FIG. 3. Cu_2OSO_4 structure obtained from X-ray diffraction.

ing monotonically with increasing temperature. In zero field a pronounced peak is found at 20 K, corresponding to a transition into a magnetically long range-ordered phase, as evidenced by other experimental measurements discussed in later sections. The peak shifts to slightly higher temperature at 9 T. In order to extract the magnetic part of the specific heat, C_{mag} , and to deduce the corresponding entropy S_{mag} , we simulate the lattice contribution from the high temperature data by taking into account one Debye (C_D) and several Einstein ($C_{E,i}$) contributions. We use a combined fit to describe the C_p and the volume of the unit cell obtained from x-ray diffraction by a phonon (lattice only) model. Similarly to what has been done in^{40,41}, the lattice contribution to the specific heat is given by $C_p = C_D + \sum_i C_{E,i}$ with :

$$C_D = 9n_D R \left(\frac{T}{\Theta_D} \right)^3 \int_0^{\Theta_D/T} \frac{x^4 e^x}{(e^x - 1)^2} dx \quad (1)$$

and

$$C_E = 3n_E R \frac{y^2 e^y}{(e^y - 1)^2}, y \equiv \Theta_E/T \quad (2)$$

Where R denotes the gas constant, Θ_D and Θ_E are the Debye and Einstein temperatures respectively. The sum $n_D + n_E$ is the total number of atoms per formula unit. The volume of the unit cell has been fitted together with the specific heat using the Debye and Einstein contributions to the internal energy. The volume of the unit cell is related to the internal energy by⁴²⁻⁴⁴:

$$V(T) = \gamma U(T)/K_0 + V_0 \quad (3)$$

Where V_0 is the cell volume at $T = 0$ K, K_0 is the bulk modulus and γ is the Grüneisen parameter. $U(T)$ is the internal energy which can be expressed in terms of the Debye and Einstein approximation as :

$$U(T) = U_D(T) + U_E(T) \quad (4)$$

$$U_D(T) = 9n_D k_B T \left(\frac{T}{\Theta_D} \right)^3 \int_0^{\Theta_D/T} \frac{x^3}{e^x - 1} dx \quad (5)$$

$$U_E(T) = \frac{3}{2} k_B \sum_i n_{E,i} \Theta_{E,i} \coth \left(\frac{\Theta_{E,i}}{2T} \right) \quad (6)$$

The best fit for both sets of data, using one Debye branch and two Einstein branches yields the characteristic temperatures : $\Theta_D = 171$ K, $\Theta_{E1} = 245$ K and $\Theta_{E2} = 939$ K with $n_D = 1$, $n_{E1} = 3$ and $n_{E2} = 4$. This fit was performed using data for temperatures larger than 70 K. The volume of the unit cell at zero Kelvin has also been fitted to be : $V_0 = 373.65 \text{ \AA}^3$, (Fig. 1).

Fig. 4 show the resulting C_{mag}/T in zero field as well as the magnetic entropy, $S_{\text{mag}}(T)$ obtained by integrating C_{mag}/T over temperature. The magnetic entropy saturates around 101(19)% of $R \ln 2$ per formula unit, which is in agreement

with the entropy of a two level spin half system. A similar analysis carried out on the 9 T data (not shown) indicates negligible field effects. The magnetic entropy is shared between short range correlations (Fig. 4, green shading) and phase transition to long range order (Fig. 4, blue shading). We estimate that 18(5)% of the magnetic entropy contributes to the phase transition.

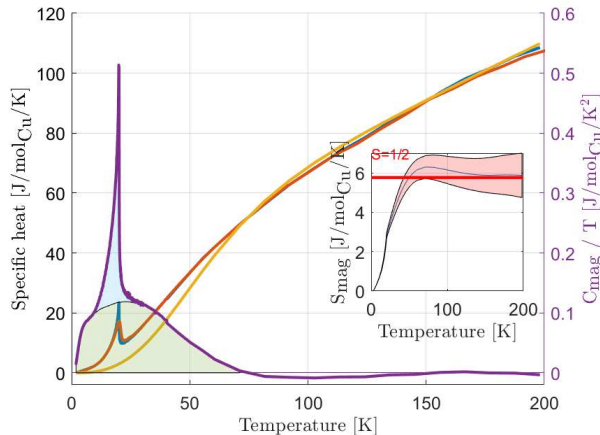


FIG. 4. Specific heat C_p as a function of temperature in zero field (blue) and 9T (red). Yellow line is the fitted lattice contribution. The purple curve (right vertical axis) shows the magnetic part of the specific heat, C_{mag}/T . The blue and green shadings represent the estimated C_{mag}/T that contributes respectively to the phase transition and to short range correlations. The inset presents the magnetic entropy, $S_{\text{mag}}(T) = \int C_{\text{mag}}(T)/TdT$. Red shading shows the confidence interval.

C. Susceptibility and magnetization

The inverse DC susceptibility measured on a single crystal, with a field of 0.1 T, pointing along the three relevant crystallographic directions : a, b, and c^* is shown in Fig. 5. The high temperature part of $\chi(T)$ fits the Curie-Weiss law, $\chi(T) = C/(T-\Theta_{\text{CW}}) + \chi_0$, where Θ_{CW} is the Curie-Weiss temperature, $C = \mu_{\text{eff}}^2/8$ and χ_0 a temperature independent diamagnetic and background term. $\mu_{\text{eff}} = g\sqrt{S(S+1)}$ is the effective magnetic moment, which is temperature independent. For a spin half system with a Landé g-factor of 2 the effective magnetic moment is worth approximately $1.7 \mu_B$. Deviations from this value can be explained by either a slightly different spin state or a g-factor different from 2, also possibly anisotropic. The fitted effective moments, Θ_{CW} and χ_0 are given in table I and the corresponding fits can be observed in Fig. 5. The Curie Weiss temperature is isotropic within errorbars and negative, which indicate dominating antiferromagnetic interactions. The g-tensor is slightly anisotropic with easy axis along b and hard axis along a. Below 20K the susceptibility steeply increases indicating a magnetic transition into a state with a ferromagnetic component. ZFC - FC splitting at low temperature is typical of weak ferromagnetic hysteresis. The magnetic transition occurring well below Θ_{CW} indicates or-

der is suppressed by fluctuations due to a combination of low dimensionality and frustration.

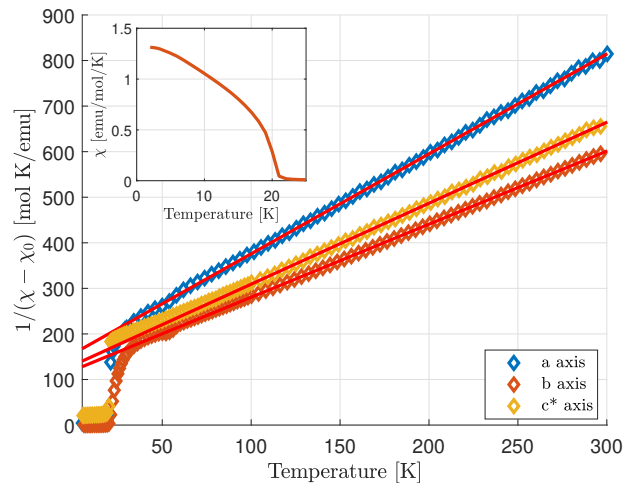


FIG. 5. Curie-Weiss fits of the high temperature susceptibility data, along the a axis (blue), b axis (red), and c^* axis (yellow). The red lines indicate the fit for each direction.

direction	Θ_{CW} [K]	χ_0	μ_{eff} [μ_B]
a	-71(4)	5.4e-05	1.91(25)
b	-75(1)	4.7e-04	2.23(25)
c^*	-70(1)	-7.6e-05	2.11(11)

TABLE I. Results of Curie-Weiss fits for measurements along a, b and c^*

Fig. 6 shows difference in the field cooled (FC) and zero field cooled (ZFC) DC magnetic susceptibility measured along the b axis, for different values of measurement field : $H = 5$ mT, $H = 10$ mT, $H = 20$ mT, $H = 50$ mT.

The susceptibility along the other two crystallographic directions (not shown) (a and c^*) show a similar temperature dependence, but with a much smaller value reached at low temperatures. We conclude that the susceptibility only grows along the b-direction and that the small signal in the a and c^* measurements is due to a small misalignment of the crystal.

Fig. 7 shows the isothermal magnetization curves for fields parallel to the b axis. For temperatures higher than 20 K, the curves are linear, indicating a paramagnetic state. Below 20 K, a small hysteresis opens. The saturation field increases when the temperature decreases and reaches 40 mT at 2 K. No similar hysteresis opens when applying the field along the c^* axis nor along the a axis (not shown). This is another indication of a ferrimagnetic ground state with a moment $\simeq 1/4 \mu_B$ pointing along the b axis. The hysteresis curve is slightly asymmetric, and displayed a slow time-dependence. This exchange-bias related phenomenon could reflect that the ferrimagnetism is the result of coupling ferromagnetic and antiferromagnetic sub-units.

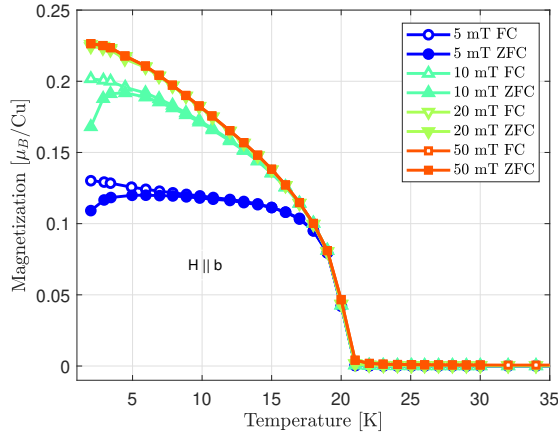


FIG. 6. Magnetization measured on a single crystal with field along the b axis highlighting Field Cooled - Zero Field Cooled separation in low fields. The strongest separation occurs at 5 mT and decreases with field.

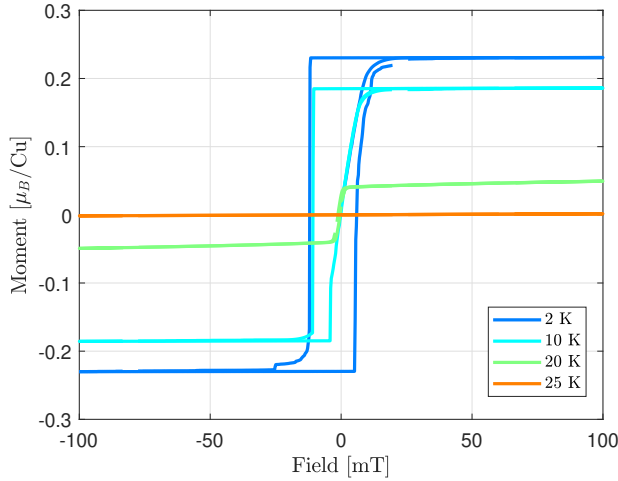


FIG. 7. Isothermal magnetization for $H \parallel b$ measured on a single crystal.

D. Neutron Diffraction

To determine the magnetic structure, neutron diffraction measurements were performed on powder samples. Fig. 8 shows in blue the data measured at 1.5 K. The magnetic scattering has been separated by measuring a powder diffraction pattern above the magnetic transition at 30 K. The subtraction of the nuclear data from the base temperature data is displayed in red in Fig. 8. Some up-down features appear due to lattice contraction, changing the Bragg peak positions.

Every magnetic contribution is located at a nuclear Bragg peak. This indicates that the magnetic propagation vector is $k=(000)$. Magnetic symmetry analysis was done for this propagation vector using the program BasIreps⁴⁵⁻⁴⁷ for the Wyckoff sites 42 (Cu_1) and 4i (Cu_2) in space group $C2/m$. Table II lists the allowed irreducible representations (Irreps)

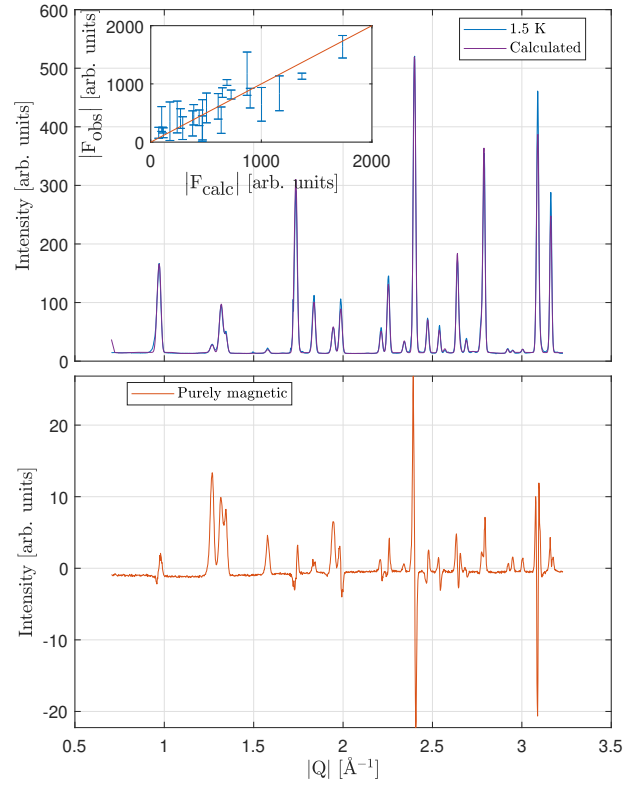


FIG. 8. Refinement of neutron diffraction data from D20: lowest temperature data measured at 1.5 K (blue), and result of the fit (purple). The purely magnetic signal (difference between data measured above and below the transition temperature) is shown in red. The inset shows the result of magnetic refinement of the data collected at ZEBRA, with Irreps Γ_1 at a base temperature of 1.5 K. The curves display the observed versus the calculated structure factors. The best fit shows good qualitative agreement with the model.

	$\text{Cu}_1 : x,y,z$	$\text{Cu}_1 : -x,y,-z$	$\text{Cu}_2 : x,y,z$	$\text{Cu}_2 : -x,y,-z$
Γ_1	(u,v,w)	(-u,v,-w)	(0 s 0)	(0 s 0)
Γ_2			(r 0 t)	(-r 0 -t)
Γ_3	(u, v, w)	(u, -v, w)	(r 0 t)	(r 0 t)
Γ_4			(0 s 0)	(0 -s 0)

TABLE II. Basis functions of irreducible representations Γ_ν for $k = (000)$. Only the real components are presented because the imaginary part is zero. The two equivalent copper sites are related through the indicated transformations.

labelled $\Gamma_1 - \Gamma_4$ and their basis vectors labelled (u,v,w) for site 1 and (r,s,t) for site 2 and shows how the magnetic moments on the symmetry related sites x,y,z and $-x,y,-z$ are constrained and transformed by the different possible Irreps.

Refinements were carried out using the Fullprof suite⁴⁵. The 30 K data were first refined to solve the nuclear structure. The scale factor obtained in this refinement was then fixed and used to refine the purely magnetic scattering of a dataset created by subtracting the 30 K data from the 1.5 K data having the same statistics. In doing so, the sensitivity for the magnetic contribution increases strongly reducing the uncertainties in the determination of the magnetic components.

	u	v	w	s	$ \vec{\mu}_{\text{Cu}_1} $	$ \vec{\mu}_{\text{Cu}_2} $
	$[\mu_B]$	$[\mu_B]$	$[\mu_B]$	$[\mu_B]$	$[\mu_B]$	$[\mu_B]$
w \neq 0	0.83(5)	-0.47(4)	0.30(9)	0.86(5)	0.98(4)	0.86(5)
w = 0	0.70(4)	-0.45(5)	0	0.91(6)	0.83(8)	0.91(6)

TABLE III. Result of fit to magnetic Irrep Γ_1 . The second row shows results if constraining the moments to the ab-plane.

In addition to the powder diffraction we also carried out a single crystal neutron diffraction experiment on the four-circles diffractometer ZEBRA, at SINQ, PSI. The crystal used turned out to present a strong mosaicity, which did not enable us to collect intensity at Bragg reflections in a systematic way and in all the directions of reciprocal space. Intensities for a set of 55 reflections were collected at a base temperature of 1.5 K as well as at 25 K to solve the nuclear structure. The result of the fit of the experimental data is presented in the inset of Fig. 8, for a choice of Irrep Γ_1 on both copper sites.

The best refinement is given by Γ_1 on both inequivalent sites. Fig. 8 shows in purple the result of the calculation of the base temperature data using the fit result. Fig. 9 shows the associated configuration of magnetic moments. The result of the fit of irreducible representation Γ_1 on both sites is presented in table III. If the Irreps are set to the result obtained by the powder diffraction experiment, then the free parameters in the single crystal refinement from Zebra can be reasonably adjusted and lead to a magnetic structure showing good agreement with the one obtained from the refinement of the powder data. The magnetic structure consists of Cu_1 antiferromagnetic chains with non colinear moments. This is the configuration that a 1D chain would adopt in magnetic field along the chain, with the field strength equal to half the saturation field. The chains are connected by Cu_2 dimers. The Cu_2 atoms in the dimer are ferromagnetically coupled. The copper atoms in the chains form an approximate 120 degrees structure with 4 spins: two Cu_2 atoms and two Cu_1 atoms belonging to the Cu_1 chains. The magnetic moments along the a and c* directions are compensated and the magnetic structure only supports a net moment along the b axis. Using values obtained from neutron diffraction in table III, we obtain the following saturation moment along the b axis : $0.23(3) \mu_B$. This moment is made up of a quarter of the sum of the moments of two Cu_1 and two Cu_2 atoms, and is in perfect agreement with the isothermal magnetization shown in Fig. 7.

Temperature dependent neutron diffraction was performed on a powder sample. Using LBF, one can extract the associated change of the lattice parameters on the whole measured range. Fig. 2 shows the relative change of the lattice parameters, which reflect the onset of magnetic order below 20 K. Fig. 10 shows the evolution of the ordered magnetic moments as a function of temperature, obtained from neutron diffraction. Solid lines correspond to power-law fits: $\mu(T) \propto (T_N - T)^{2\beta}$. The fit of the data yields $T_N = 19.7(07)$ K, shared by the two sites, and $\beta = 0.12(1)$ for site 1 and $\beta = 0.13(2)$ for site 2.

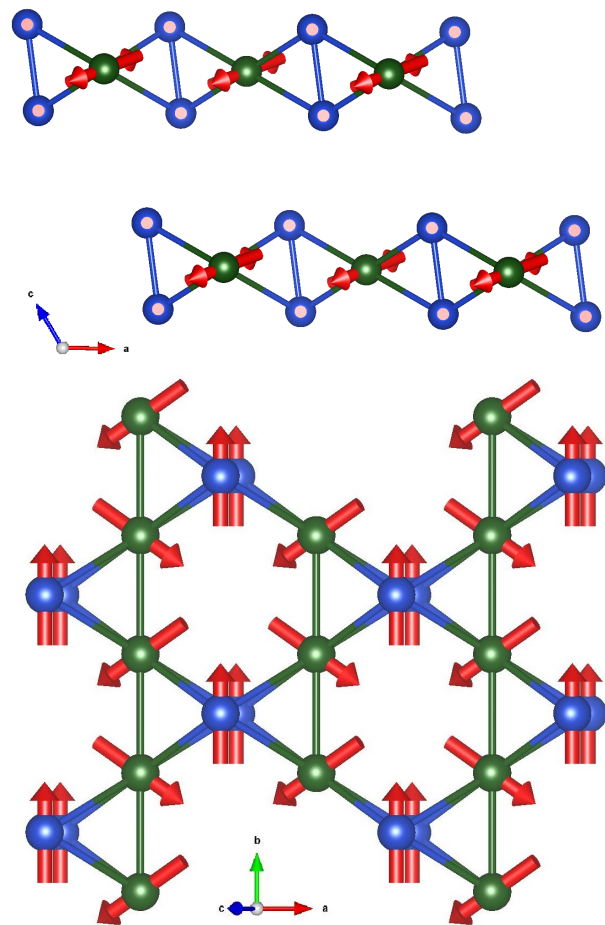


FIG. 9. Magnetic structure of Cu_2OSO_4 refined with Irrep Γ_1 on both sites. Copper site one is shown in green while copper site two is shown in blue.

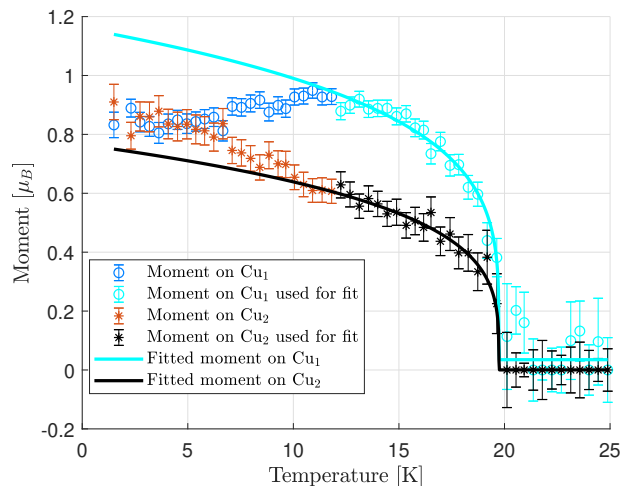


FIG. 10. Temperature dependence of magnetic refinements with Irreps Γ_1 . The solid lines are a power-law fit to the magnetic moment on each site : $\mu(T) \propto (T_N - T)^{2\beta}$. The fitting of the power law behavior has been performed over the specified data range (black and cyan).

IV. DISCUSSION

The ordered structure determined from the neutron powder diffraction is fully consistent with exchange paths present in this compound. A close inspection of the structure reveals which are the most relevant superexchange paths. The pathway between two Cu_2 ions contains oxygen ions, forming the $\text{Cu}_2 - \text{O} - \text{Cu}_2$ angle $\sim 93.0^\circ$ which favors a ferromagnetic J_{22} according to the Goodenough-Kanamori-Anderson (GKA) rules. On the other hand the $\text{Cu}_1 - \text{O} - \text{Cu}_1$ angle between two nearest-neighbor Cu_1 atoms is 114.9° . This falls well in the range of values predicted by GKA rules to favor antiferromagnetic J_{11} interactions. For the coupling between two inequivalent copper sites there are two distinct superexchange paths, one forming a $\text{Cu}_1 - \text{O} - \text{Cu}_2$ angle of 104.9° while the other one is 117.3° . Such values are again consistent with antiferromagnetic couplings (J_{21a} and J_{21b} , respectively).

Additional exchange pathways exist and involve sulphur tetrahedra, more precisely $\text{Cu} - \text{O} - \text{O} - \text{Cu}$ super-superexchange interactions. They provide a coupling between Cu_2 dimers as well as an overall inter-planar coupling which eventually leads to the observed long-range order. It is a non-trivial task to estimate their relative strength to super-exchange in-plane coupling. Future inelastic neutron scattering experiments and modelling of dispersion relations could give us an indication which interactions are the most relevant for the long-range order in $\text{Cu}_2 - \text{O} - \text{Cu}_2$.

As a final note, an antisymmetric Dzyaloshinskii-Moriya (DM) interaction has been indicated to exist in this compound⁴⁸, compatible with crystal symmetry. Its magnitude has been estimated to be $D \sim 7$ K. If we take $\theta_{CW} \sim 70$ K as an estimate for J , we arrive at $D/J \gtrsim 0.1$. For the Kagomé lattice, DM interactions have been predicted to cause a quantum phase transition stabilizing 120° order above $D_c = 0.1J$ ^{49,50}. Given the similar relative order of D in Cu_2OSO_4 , it is possible that this interaction is partly responsible for the 120° order and as a consequence Cu_2OSO_4 may be close to a quantum phase transition, which could possibly be reached by tuning the system through pressure or chemical

substitution.

V. CONCLUSION

In summary, we have presented a detailed study of the magnetic properties of Cu_2OSO_4 . We confirmed that the structure of Cu_2OSO_4 does not change upon cooling and that the ground state corresponds to a $S = 1/2$ system. The Curie Weiss temperatures give an idea of the order of magnitude of the magnetic couplings involved in the system, 70 K, however, the system undergoes a second order magnetic phase transition to a magnetically long range ordered state only below 20 K. Neutron scattering reveals that the ground state corresponds roughly to 120° order. The fact that this specific magnetic structure turns out to be the ground state, even though one third of the sites in the Kagomé-like lattice is replaced by ferromagnetic dimers is interesting. The rather small entropy linked to the transition suggest that there might be interesting dynamics related to the formation of ferromagnetic pairs and 120° triangles and subsequent alignment of these units. We hope this study will stimulate further theoretical and experimental studies of the dynamics in this new triangular motif model compound.

VI. ACKNOWLEDGMENTS

V. Y. F. thanks P. Babkevich for his help with the refinement of diffraction data, and F. Mila for stimulating discussions. We acknowledge the Paul Scherrer Institut, Villigen, Switzerland for provision of synchrotron radiation beamtime at beamline MS-X04SA of the SLS. This work is partially based on experiments performed at the Swiss spallation neutron source SINQ, Paul Scherrer Institute, Villigen, Switzerland, at the STFC ISIS Facility⁵¹ and at the Institut Laue-Langevin⁵². A portion of this research used resources at the High Flux Isotope Reactor, a DOE Office of Science User Facility operated by the Oak Ridge National Laboratory. This work was supported by the Swiss National Science Foundation (SNSF) grant No. 188648.

* ivica.zivkovic@epfl.ch

† henrik.ronnow@epfl.ch

¹ A. Olariu, P. Mendels, F. Bert, B. G. Ueland, P. Schiffer, R. F. Berger, and R. J. Cava, "Unconventional Dynamics in Triangular Heisenberg Antiferromagnet NaCrO_2 ," *Physical Review Letters*, vol. 97, Oct. 2006.

² Y. Shirata, H. Tanaka, A. Matsuo, and K. Kindo, "Experimental Realization of a Spin-1/2 Triangular-Lattice Heisenberg Antiferromagnet," *Physical Review Letters*, vol. 108, Jan. 2012.

³ Y. Kojima, M. Watanabe, N. Kurita, H. Tanaka, A. Matsuo, K. Kindo, and M. Avdeev, "Quantum magnetic properties of the spin-1/2 triangular-lattice antiferromagnet $\text{Ba}_2\text{La}_2\text{CoTe}_2\text{O}_{12}$," *Physical Review B*, vol. 98, Nov. 2018.

⁴ P. Anderson, "Resonating valence bonds: A new kind of insulator?," *Materials Research Bulletin*, vol. 8, no. 2, pp. 153 – 160, 1973.

⁵ P. Fazekas and P. W. Anderson, "On the ground state properties of the anisotropic triangular antiferromagnet," *Philosophical Magazine*, vol. 30, pp. 423–440, Aug. 1974.

⁶ M. Collins and O. Petrenko, "Triangular antiferromagnets. Can J Phys 75:605," *Canadian Journal of Physics*, vol. 75, pp. 605–, 09 1997.

⁷ F. Ferrari, A. Parola, S. Sorella, and F. Becca, "Dynamical structure factor of the $J_1 - J_2$ Heisenberg model in one dimension: The variational Monte Carlo approach," *Physical Review B*, vol. 97, June 2018.

- ⁸ O. Mustonen, S. Vasala, E. Sadrollahi, K. Schmidt, C. Baines, H. Walker, I. Terasaki, F. Litterst, E. Baggio-Saitovitch, and M. Karppinen, “Spin-liquid-like state in a spin-1/2 square-lattice antiferromagnet perovskite induced by d 10–d 0 cation mixing,” *Nature communications*, vol. 9, no. 1, p. 1085, 2018.
- ⁹ M. P. Shores, E. A. Nytko, B. M. Bartlett, and D. G. Nocera, “A Structurally Perfect $S = 1/2$ Kagomé Antiferromagnet,” *Journal of the American Chemical Society*, vol. 127, pp. 13462–13463, Oct. 2005.
- ¹⁰ P. Mendels and F. Bert, “Quantum kagome frustrated antiferromagnets: One route to quantum spin liquids,” *Comptes Rendus Physique*, vol. 17, pp. 455–470, Mar. 2016.
- ¹¹ J. S. Helton, K. Matan, M. P. Shores, E. A. Nytko, B. M. Bartlett, Y. Yoshida, Y. Takano, A. Suslov, Y. Qiu, J.-H. Chung, D. G. Nocera, and Y. S. Lee, “Spin Dynamics of the Spin-1/2 Kagome Lattice Antiferromagnet $\text{ZnCu}_3(\text{OH})_6\text{Cl}_2$,” *Physical Review Letters*, vol. 98, Mar. 2007.
- ¹² A. Zorko, S. Nellutla, J. van Tol, L. C. Brunel, F. Bert, F. Duc, J.-C. Trombe, M. A. de Vries, A. Harrison, and P. Mendels, “Dzyaloshinsky-Moriya Anisotropy in the Spin-1/2 Kagome Compound $\text{ZnCu}_3(\text{OH})_6\text{Cl}_2$,” *Physical Review Letters*, vol. 101, July 2008.
- ¹³ S. Depenbrock, I. P. McCulloch, and U. Schollwock, “Nature of the Spin-Liquid Ground State of the $S = 1/2$ Heisenberg Model on the Kagome Lattice,” *Physical Review Letters*, vol. 109, Aug. 2012.
- ¹⁴ F. Mila, “Low-Energy Sector of the $S = 1/2$ Kagome Antiferromagnet,” *Physical Review Letters*, vol. 81, pp. 2356–2359, Sept. 1998.
- ¹⁵ R. R. P. Singh and D. A. Huse, “Ground state of the spin-1/2 kagome-lattice Heisenberg antiferromagnet,” *Physical Review B*, vol. 76, Nov. 2007.
- ¹⁶ S. Yan, D. A. Huse, and S. R. White, “Spin-Liquid Ground State of the $S = 1/2$ Kagome Heisenberg Antiferromagnet,” *Science*, vol. 332, no. 6034, pp. 1173–1176, 2011.
- ¹⁷ S. Depenbrock, I. P. McCulloch, and U. Schollwock, “Nature of the Spin-Liquid Ground State of the $S = 1/2$ Heisenberg Model on the Kagome Lattice,” *Physical Review Letters*, vol. 109, Aug. 2012.
- ¹⁸ M. Hermele, Y. Ran, P. A. Lee, and X.-G. Wen, “Properties of an algebraic spin liquid on the kagome lattice,” *Physical Review B*, vol. 77, June 2008.
- ¹⁹ L. Clark, J. C. Orain, F. Bert, M. A. De Vries, F. H. Aidoudi, R. E. Morris, P. Lightfoot, J. S. Lord, M. T. F. Telling, P. Bonville, J. P. Attfield, P. Mendels, and A. Harrison, “Gapless Spin Liquid Ground State in the $S = 1/2$ Vanadium Oxyfluoride Kagome Antiferromagnet $[\text{NH}_4]_2[\text{C}_7\text{H}_{14}\text{N}][\text{V}_7\text{O}_6\text{F}_{18}]$,” *Physical Review Letters*, vol. 110, May 2013.
- ²⁰ Y. Iqbal, F. Becca, S. Sorella, and D. Poilblanc, “Gapless spin-liquid phase in the kagome spin-1/2 Heisenberg antiferromagnet,” *Physical Review B*, vol. 87, Feb. 2013.
- ²¹ M. Fu, T. Imai, T.-H. Han, and Y. S. Lee, “Evidence for a gapped spin-liquid ground state in a kagome Heisenberg antiferromagnet,” *Science*, vol. 350, no. 6261, pp. 655–658, 2015.
- ²² M. Takano, T. Shinjo, and T. Takada, “On the spin arrangement in kagome lattice of antiferromagnetic $\text{KFe}_3(\text{OH})_6(\text{SO}_4)_2$,” *Journal of the Physical Society of Japan*, vol. 30, no. 4, pp. 1049–1053, 1971.
- ²³ Y. Okamoto, H. Yoshida, and Z. Hiroi, “Vesignieite $\text{BaCu}_3\text{V}_2\text{O}_8(\text{OH})_2$ as a Candidate Spin-1/2 Kagome Antiferromagnet,” *Journal of the Physical Society of Japan*, vol. 78, p. 033701, Mar. 2009.
- ²⁴ T. H. Han, J. S. Helton, S. Chu, A. Prodi, D. K. Singh, C. Mazzoli, P. Müller, D. G. Nocera, and Y. S. Lee, “Synthesis and characterization of single crystals of the spin-1/2 kagome-lattice antiferromagnets $\text{Zn}_x\text{Cu}_{4-x}(\text{OH})_6\text{Cl}_2$,” *Physical Review B*, vol. 83, Mar. 2011.
- ²⁵ B. Martínez, F. Sandiumenge, A. Rouco, A. Labarta, J. Rodríguez-Carvajal, M. Tovar, M. Causa, S. Galfí, and X. Obradors, “Magnetic dilution in the strongly frustrated kagome antiferromagnet $\text{SrGa}_{12-x}\text{Cr}_x\text{O}_{19}$,” *Physical Review B*, vol. 46, pp. 10786–10792, Nov. 1992.
- ²⁶ Z. Hiroi, M. Hanawa, N. Kobayashi, M. Nohara, H. Takagi, Y. Kato, and M. Takigawa, “Spin-1/2 kagome-like lattice in volborthite $\text{Cu}_3\text{V}_2\text{O}_7(\text{OH})_2\cdot 2\text{H}_2\text{O}$,” *Journal of the Physical Society of Japan*, vol. 70, no. 11, pp. 3377–3384, 2001.
- ²⁷ P. Mendels and F. Bert, “Quantum Kagome Antiferromagnet $\text{ZnCu}_3(\text{OH})_6\text{Cl}_2$,” *Journal of the Physical Society of Japan*, vol. 79, p. 011001, Jan. 2010.
- ²⁸ M. Wolf and K. D. Schotte, “Ising model with competing next-nearest-neighbour interactions on the Kagome lattice,” *Journal of Physics A: Mathematical and General*, vol. 21, pp. 2195–2209, may 1988.
- ²⁹ O. Cépas, C. M. Fong, P. W. Leung, and C. Lhuillier, “Quantum phase transition induced by Dzyaloshinskii-Moriya interactions in the kagome antiferromagnet,” *Physical Review B*, vol. 78, Oct. 2008.
- ³⁰ Y. Huh, L. Fritz, and S. Sachdev, “Quantum criticality of the kagome antiferromagnet with Dzyaloshinskii-Moriya interactions,” *Physical Review B*, vol. 81, Apr. 2010.
- ³¹ B. Dalla Piazza, M. Mourigal, N. B. Christensen, G. J. Nilsen, P. Tregenna-Piggott, T. G. Perring, M. Enderle, D. F. McMorrow, D. A. Ivanov, and H. M. Rønnow, “Fractional excitations in the square-lattice quantum antiferromagnet,” *Nature Physics*, vol. 11, pp. 62–68, Jan 2015.
- ³² E. Flügel-Kahler, “Die Kristallstruktur von Dolerophanit, $\text{Cu}_2\text{O}(\text{SO}_4)$,” *Acta Crystallographica*, vol. 16, pp. 1009–1014, Oct 1963.
- ³³ L. Bald, M. Spiess, R. Gruehn, and T. Kohlmann, “Beiträge zum thermischen Verhalten von Sulfaten. VI. Zum chemischen Transport von CuSO_4 , Cu_2OSO_4 und CuO ,” *Zeitschrift für anorganische und allgemeine Chemie*, vol. 498, pp. 153–160, Mar. 1983.
- ³⁴ M. Belaiche, M. Drillon, J. Aride, A. Boukharis, T. Biaz, and P. Legoll, “Application du modèle Heisenberg à la chaîne ferromagnétique d’ions $\text{Cu}(\text{II})$ dans Cu_2OSO_4 ,” *J Chim Phys*, pp. 1713–1719, 1991.
- ³⁵ M. Drillon, M. Belaiche, and J. Heintz, “G. vileneuve”, a. boukhari” and j. aride”, *Organic and Inorganic Low-Dimensional Crystalline Materials*, vol. 168, p. 421, 2013.
- ³⁶ N. Takahashi, S. Okubo, H. Ohta, T. Sakurai, M. Fujisawa, and H. Kikuchi, “Dzyaloshinsky-Moriya Interaction Estimated by AFMR of Kagome Like Substance $\text{Cu}_2\text{O}(\text{SO}_4)$ Observed at 1.8K,” *Journal of Physics: Conference Series*, vol. 400, p. 032097, Dec. 2012.
- ³⁷ T. Asai, H. Saheki, and R. Kiriyama, “Magnetic Studies on Basic Salts of Copper, Dicopper Arsenate Hydroxide, Dicopper Hydroxide Phosphate, and Dicopper Oxide Sulfate,” *Bulletin of the Chemical Society of Japan*, vol. 52, pp. 310–314, Feb. 1979.
- ³⁸ P. R. Willmott, D. Meister, S. J. Leake, M. Lange, A. Bergamaschi, M. Böge, M. Calvi, C. Cancellieri, N. Casati, A. Cervellino, Q. Chen, C. David, U. Flechsig, F. Gozzo, B. Henrich, S. Jäggi-Spielmann, B. Jakob, I. Kalichava, P. Karvinen, J. Krempasky, A. Lüdeke, R. Lüscher, S. Maag, C. Quitmann, M. L. Reinle-Schmitt, T. Schmidt, B. Schmitt, A. Streun, I. Vartiainen, M. Vitins, X. Wang, and R. Wulfschleger, “The Materials Science beamline upgrade at the Swiss Light Source,” *Journal of Synchrotron Radiation*, vol. 20, pp. 667–682, Sep 2013.

- ³⁹ K. Momma and F. Izumi, “VESTA3 for three-dimensional visualization of crystal, volumetric and morphology data,” *Journal of Applied Crystallography*, vol. 44, pp. 1272–1276, Dec 2011.
- ⁴⁰ L. Yang, M. Jeong, P. Babkevich, V. M. Katukuri, B. Náfrádi, N. E. Shaik, A. Magrez, H. Berger, J. Schefer, E. Ressouche, M. Kriener, I. Živković, O. V. Yazyev, L. Forró, and H. M. Rønnow, “J 1 - J 2 square lattice antiferromagnetism in the orbitally quenched insulator MoOPO 4,” *Physical Review B*, vol. 96, July 2017.
- ⁴¹ H. Papi, V. Y. Favre, H. Ahmadvand, M. Alaei, M. Khondabi, D. Sheptyakov, L. Keller, P. Kameli, I. Živković, and H. M. Rønnow, “Magnetic and structural properties of Ni-substituted magnetoelectric Co₄Nb₂O₉,” *Phys. Rev. B*, vol. 100, p. 134408, Oct 2019.
- ⁴² P. Bag, P. R. Baral, and R. Nath, “Cluster spin-glass behavior and memory effect in Cr 0.5 Fe 0.5 Ga,” *Physical Review B*, vol. 98, Oct. 2018.
- ⁴³ S. Pakhira, C. Mazumdar, R. Ranganathan, S. Giri, and M. Avdeev, “Large magnetic cooling power involving frustrated antiferromagnetic spin-glass state in R 2 NiSi 3 (R = Gd , Er),” *Physical Review B*, vol. 94, Sept. 2016.
- ⁴⁴ D. W. Rogers, *Einstein’s ”Other” Theory: The Planck-Bose-Einstein Theory of Heat Capacity*. Princeton University Press, 2005.
- ⁴⁵ J. Rodríguez-Carvajal, “Recent advances in magnetic structure determination by neutron powder diffraction,” *Physica B: Condensed Matter*, vol. 192, no. 1, pp. 55 – 69, 1993.
- ⁴⁶ C. Ritter, “Neutrons Not Entitled to Retire at the Age of 60: More than Ever Needed to Reveal Magnetic Structures,” in *Solid Compounds of Transition Elements*, vol. 170 of *Solid State Phenomena*, pp. 263–269, Trans Tech Publications Ltd, 3 2011.
- ⁴⁷ J. Rodríguez-Carvajal, “BASIREPS: a program for calculating irreducible representations of space groups and basis functions for axial and polar vector properties, Part of the FullProf Suite of programs available at: www.ill.eu/sites/fullprof/,”
- ⁴⁸ N. Takahashi, S. Okubo, H. Ohta, T. Sakurai, M. Fujisawa, and H. Kikuchi, “Dzyaloshinsky-Moriya Interaction Estimated by AFMR of Kagome Like Substance Cu₂O(SO₄) Observed at 1.8K,” *Journal of Physics Conference Series*, vol. 400, pp. 2097–, 12 2012.
- ⁴⁹ I. Rousochatzakis, S. R. Manmana, A. M. Läuchli, B. Normand, and F. Mila, “Dzyaloshinskii-Moriya anisotropy and nonmagnetic impurities in the $s = \frac{1}{2}$ kagome system ZnCu₃(OH)₆Cl₂,” *Phys. Rev. B*, vol. 79, p. 214415, Jun 2009.
- ⁵⁰ O. Cépas, C. M. Fong, P. W. Leung, and C. Lhuillier, “Quantum phase transition induced by Dzyaloshinskii-Moriya interactions in the kagome antiferromagnet,” *Phys. Rev. B*, vol. 78, p. 140405, Oct 2008.
- ⁵¹ H. M. Rønnow, “Structure and magnetic order of the diamond-kagome planar compound cu₂oso₄,” *STFC ISIS facility*, 2018.
- ⁵² H. M. Rønnow, “Magnetic order of the diamond-kagomé planar compound cu₂oso₄,” *Institut Laue-Langevin (ILL): Grenoble*, 2018.